

Spin-wave excitations in presence of nanoclusters of magnetic impurities

Akash Chakraborty

*Institut für Theoretische Festkörperphysik,
Karlsruhe Institute of Technology, 76128 Karlsruhe, Germany and
School of Engineering and Science, Jacobs University Bremen,
Campus Ring 1, 28759 Bremen, Germany*

Paul Wenk

Institut I - Theoretische Physik, Universität Regensburg, 93040 Regensburg, Germany

Stefan Kettemann

*Division of Advanced Materials Science,
Pohang University of Science and Technology (POSTECH),
Pohang 790-784, South Korea and
School of Engineering and Science, Jacobs University Bremen,
Campus Ring 1, 28759 Bremen, Germany*

Richard Bouzerar and Georges Bouzerar

*Institut Néel, CNRS, Département MCBT, 25 avenue des Martyrs,
B.P. 166, 38042 Grenoble Cedex 09, France*

(Dated: November 21, 2018)

Abstract

Nanoscale inhomogeneities and impurity clustering are often found to drastically affect the magnetic and transport properties in disordered/diluted systems, giving rise to rich and complex phenomena. However, the physics of these systems still remains to be explored in more details as can be seen from the scarce literature available. We present a detailed theoretical analysis of the effects of nanoscale inhomogeneities on the magnetic excitation spectrum in diluted systems. The calculations are performed on relatively large systems (up to $N=66^3$). It is found that even low concentrations of inhomogeneities have drastic effects on both the magnon density of states and magnon excitations. These effects become even more pronounced in the case of short ranged magnetic interactions between the impurities. In contrast to the increase of critical temperatures T_C reported in previous studies, the spin-stiffness D is systematically suppressed in the presence of nanoscale inhomogeneities. Moreover D is found to strongly depend on the inhomogeneities' concentration, their size, as well as the range of the magnetic interactions. We believe that this detailed numerical work could initiate future experimental studies to probe this rich physics with the most appropriate tool, Inelastic Neutron Scattering (INS).

PACS numbers: 75.30.Ds, 73.21.-b, 75.50.Pp

Disordered magnetic systems, such as transition metal alloys^{1–3}, diluted magnetic semiconductors (DMSs)^{4–6}, diluted magnetic oxides (DMOs)^{7,8}, and manganites^{9–11} have continued to attract a great deal of attention ever since their respective discoveries. The prospects of these materials for novel spintronic devices led to a plethora of work from both the experimental as well as the theoretical point of view. For a long time the major focus of spintronics research was mostly on homogeneously diluted systems (with magnetic impurities distributed randomly on the host lattice), which were believed to give rise to the much coveted room-temperature ferromagnetism. For that purpose huge efforts to grow systems as “clean” as possible are made. However, in contrast to the common belief, this does not systematically appear to be the optimal route to room-temperature ferromagnetism. For instance, in homogeneously or well-annealed Mn doped III-V DMSs it has been impossible, so far, to go beyond the critical temperature of 140 K for 5% Mn^{12–14}.

These findings led people to look into other possible avenues in the ultimate quest for the room-temperature phenomenon. Transmission electron microscopy (TEM) experiments revealed the presence of coherent Mn-rich spherical nanocrystals in (Ga,Mn)As^{15,16}, which exhibited a Curie temperature of \sim 360 K. Similar nanoscale clusters were also reportedly observed in other diluted materials like (Ge,Mn)^{17–19} and (Zn,Co)O²⁰, exhibiting critical temperatures in excess of 300 K. The nanoscale spinodal decomposition into regions with high and low concentration of magnetic ions was speculated to be the possible reason for the apparently high Curie temperatures in these compounds. Nanoscale inhomogeneities have also often been detected in other families of compounds. In manganites, inhomogeneities arise due to the interplay between the charge, spin, orbital, and lattice degrees of freedom, leading to the coexistence of metallic and insulating phases. For example, scanning tunneling spectroscopy (STS) images of $\text{La}_{1-x}\text{Ca}_x\text{MnO}_3$ revealed a clear phase separation just below the critical temperature²¹. It is widely believed that the phase separation is at the origin of the well known colossal magneto-resistance (CMR) effect^{22,23}. In high T_C superconductors experimental studies often indicate the crucial role of inhomogeneities^{24–26}. For example in Ref. 26, it was found that regions with weak superconductivity can persist to higher temperatures if bordered by regions of strong superconductivity. The possibility of increasing the maximum transition temperature by controlled distribution of the dopants has also been suggested.

Despite the existence of numerous experimental studies, the effects of nanoscale inhomogenei-

geneities in disordered and diluted systems still remain largely unexplored on the theoretical front. Because of the large supercells required density functional theory (DFT) based calculations for inhomogeneous systems are considerably difficult. For the same reason the essentially exact Monte Carlo studies are unfortunately incapable to deal with these systems. Moreover the crucial importance of both thermal and transverse fluctuations calls for the inevitable need of an exact treatment of the disorder effects, which implies a real space treatment. Recently using a real-space RPA approach, able to handle considerably large system sizes, it has been demonstrated that nanoscale inhomogeneities can lead to a dramatic increase of the Curie temperatures²⁷. The question which naturally arises is how impurity clustering affects the spin excitation spectrum? Indeed the spin-wave excitations provide valuable insight into the underlying spin dynamics of the system. Inelastic neutron scattering is a powerful experimental tool in this context, as the dispersion relation and the magnon damping can be measured directly and accurately. In contrast to non-dilute systems, such as manganites^{28,29}, cobaltites^{30,31}, multiferroics^{32,33}, pnictides^{34,35}, etc., one can find very few detailed studies³⁶ devoted to spin dynamics in dilute magnetic systems. Note that till now no experimental data has been reported for spin excitations in III-V DMSs, such as (Ga,Mn)As.

The aim of the current work is to provide such a detailed theoretical account of the spin excitation spectrum of diluted magnetic systems in the presence of nanoscale inhomogeneities. We show that nanoclusters of magnetic impurities can have drastic effects on the magnon density of states (DOS), the dynamical spectral function, as well as the spin-stiffness in these systems, when compared to the homogeneously diluted case. In our calculations, we have assumed for the lattice a simple cubic structure with periodic boundary conditions. In order to avoid additional parameters, the total concentration of impurities in the whole system is fixed to $x=0.07$. The inhomogeneities are assumed to be spherical of radii r_0 and the concentration inside each of these nanospheres is denoted by x_{in} . For simplicity we also fix $x_{in}=0.8$ for all cases considered in this study. We define the concentration of nanospheres in the system as $x_{ns} = N_S/N$, where N_S is the total number of sites included in all the nanospheres and $N = L^3$ is the total number of sites. A variable $P_N = (x_{in}/x)x_{ns}$, is used to represent the percentage of total impurities contained within the nanospheres. For a particular disorder configuration the nanospheres are distributed in a random manner on the lattice, the only restriction imposed is to avoid any overlapping between them.

We start with a Hamiltonian describing N_{imp} interacting spins randomly distributed on a lattice of N sites, which is given by the diluted random Heisenberg model

$$H_{Heis} = - \sum_{i,j} J_{ij} p_i p_j \mathbf{S}_i \cdot \mathbf{S}_j \quad (1)$$

where the sum ij runs over all sites and the random variable p_i is 1 if the site is occupied by an impurity, otherwise it is 0. The above Hamiltonian (Eq.1) is treated within the self-consistent local random phase approximation (SC-LRPA), which is a semi-analytical approach based on finite temperature Green's functions. Within this approach, the retarded Green's functions are defined as $G_{ij}^c(\omega) = \int_{-\infty}^{+\infty} G_{ij}^c(t) e^{i\omega t} dt$, where $G_{ij}^c(t) = -i\theta(t) \langle [S_i^+(t), S_j^-(0)] \rangle$, ($\langle \dots \rangle$ denotes the thermal average). This describes the transverse spin fluctuations and the index "c" denotes the disorder configuration. After performing the Tyablicov decoupling of the higher-order Green's functions which appear in the equation of motion of $G_{ij}^c(\omega)$ one gets,

$$G_{ij}^c(\omega) = \sum_{\alpha} \frac{2\langle S_j^z \rangle}{\omega - \omega_{\alpha}^c + i\epsilon} \langle i | \Psi_{\alpha}^{R,c} \rangle \langle \Psi_{\alpha}^{L,c} | j \rangle \quad (2)$$

where $\langle S_j^z \rangle$ are the local magnetizations which have to be calculated self-consistently. $|\Psi_{\alpha}^{R,c}\rangle$ and $|\Psi_{\alpha}^{L,c}\rangle$ are respectively the right and left eigenvectors, associated with the same eigenvalue ω_{α}^c of the effective Hamiltonian \mathbf{H}_{eff}^c , whose matrix elements are given by

$$(\mathbf{H}_{eff}^c)_{ij} = -\langle S_i^z \rangle J_{ij} + \delta_{ij} \sum_l \langle S_l^z \rangle J_{lj} \quad (3)$$

At finite T , \mathbf{H}_{eff}^c is non-Hermitian (real non-symmetric) but it is bi-orthogonal³⁷. Hence one needs to define the left and right eigenvectors of the effective Hamiltonian. However, since in the present case all calculations are performed at $T = 0$ K, the matrix \mathbf{H}_{eff}^c is real symmetric and the left and right eigenvectors are identical. For more details on the SC-LRPA approach one can see for example Refs. 5,38,39. The SC-LRPA was previously successfully implemented to calculate the magnetic excitation spectra in the nearest-neighbor diluted Heisenberg model⁴⁰ as well as in the case of optimally annealed (Ga,Mn)As⁴¹. In the latter case, an especially good agreement with experiments^{42,43} was also found.

Now it is well known from first principles based studies as well as model calculations that the exchange couplings in III-V DMS compounds are relatively short-ranged and exponentially decaying in nature^{41,44,45}. Thus, without any loss of generality, we have assumed the interactions between the magnetic impurities to be of the exponential form $J_{ij} = J_0 \exp(-|\mathbf{r}_i - \mathbf{r}_j|/\lambda)$, where λ is the damping parameter. For this damping parameter, we focus here

on two particular values, $\lambda = a$ and $a/2$ (a is the lattice spacing), corresponding to relatively long-ranged and short-ranged couplings respectively. In fact it was only recently shown that just varying λ within this scale can give rise to rather spectacular effects on the Curie temperatures in these inhomogeneous diluted systems²⁷. Our current goal is to provide a detailed analysis of the effects of nanoscale inhomogeneities, in the presence of these interactions, on the dynamical magnetic properties of diluted systems.

We first start with the calculation of the magnon DOS for the homogeneously diluted case. The average magnon DOS is given by $\rho_{avg}(\omega) = \frac{1}{N_{imp}} \sum_i \langle \rho_i^c(\omega) \rangle_c$, where $\rho_i^c(\omega)$ is the local magnon DOS, which reads $\rho_i^c(\omega) = -\frac{1}{2\pi \langle S_i^z \rangle} \text{Im}G_{ii}^c(\omega)$. In what follows $\langle \dots \rangle_c$ denotes the average over disorder configurations. Figure 1 shows ρ_{avg} as a function of the energy ω , for the two different values of λ mentioned above. The average over disorder is performed for a few hundred configurations in all the following calculations. ρ_{avg} is found to exhibit a regular Gaussian-like shape for the case of $\lambda=a$. The broad peak is located at $0.42W$ with a half-width of about $0.36W$ (W is the magnon excitation bandwidth). For longer ranged couplings, ρ_{avg} remains essentially similar to that of $\lambda = a$. On the other hand, for short-ranged couplings ($\lambda = a/2$), ρ_{avg} has a more irregular and richer structure. The peak in ρ_{avg} is now located at much lower energy, $0.06W$, and a clear long tail extending toward the high energies with multiple shoulders appears. These additional features result from clusters of impurities weakly coupled to the rest of the system. These shoulders become even more pronounced for shorter ranged interactions. It is interesting to note that a similar kind of magnon DOS was obtained in the case of (Ga,Mn)As⁴¹. However, in Ref. 41 the exchange couplings used had been directly calculated from the “*V-J*” model. It has been found that $\lambda = a/3$ provides a very good fit for these couplings.

In order to analyze the effects of inhomogeneities, we calculate in addition to ρ_{avg} , the local magnon DOS inside (ρ_{in}) and outside (ρ_{out}) the nanospheres. Unlike ρ_{avg} , the local DOS contains information on the nature of the magnon states. We consider the particular case of nanospheres with fixed radii $r_0=2a$, concentration inside $x_{in}=0.8$, and four different concentrations of nanospheres x_{ns} . The results for $\lambda=a$ are depicted in Fig. 2. Let us first focus on ρ_{avg} . From Fig. 2(a), we immediately notice that a relatively small concentration of inhomogeneities ($x_{ns} \sim 0.02$) causes a significant change in the magnon DOS. Indeed, in comparison to the homogeneous case, the excitations spectrum bandwidth is now doubled, and ρ_{avg} has a bimodal structure, with a broader peak at higher energies. With increasing

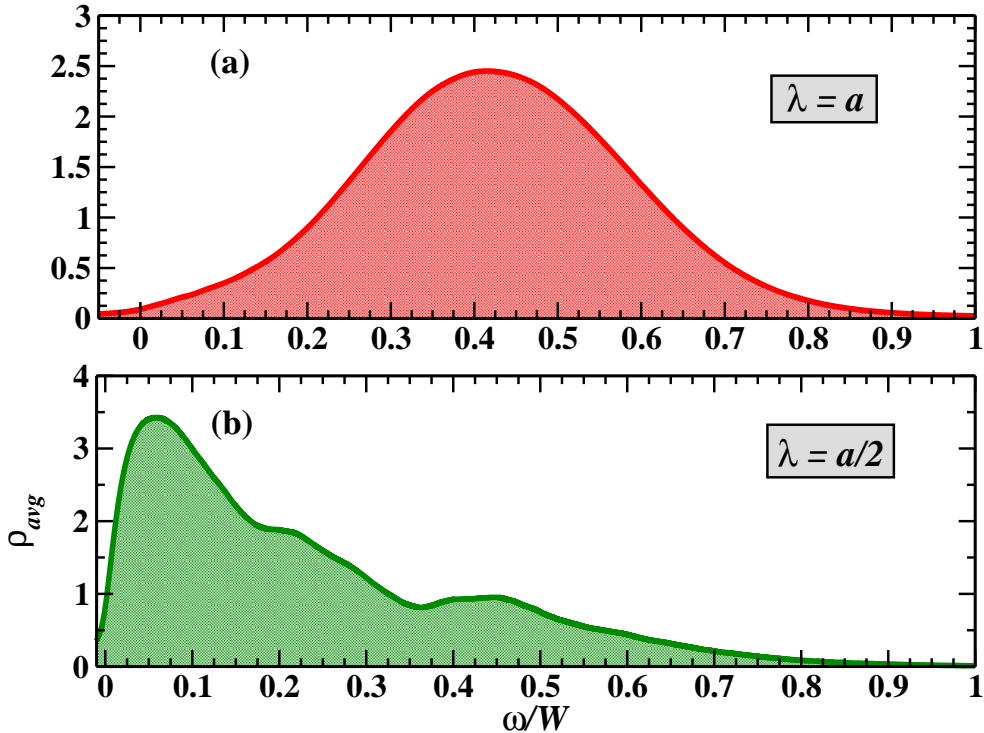


FIG. 1: (Color online) Average magnon DOS corresponding to the homogeneous case for (a) $\lambda=a$, and (b) $\lambda=a/2$. The average concentration is $x=0.07$. The x axis is in units of ω/W , where W is the magnon spectrum bandwidth. $W \approx 4J_0$ and $0.8J_0$, for $\lambda=a$ and $a/2$ respectively. The system size is $N=56^3$.

x_{ns} , we observe a gradual transfer of weight from the low to high energy peak. The low energy peak shifts to smaller energies which is consistent with the decrease in the concentration of impurities outside the nanospheres. In order to have a better understanding of the features seen in ρ_{avg} , we now analyze ρ_{in} and ρ_{out} . We observe that ρ_{in} remains unchanged in all cases and exhibit a very small weight from 0 to $0.7W$. Thus the high energy peak seen in ρ_{avg} can clearly be attributed to the nanocluster modes. A careful analysis of a single isolated cluster reveals that the first non-zero eigenmodes are located at $0.7W$, which explains the very small weight in ρ_{in} below this value. Note that in Fig. 2(a), the shaded regions correspond to the discrete spectrum of an isolated single nanosphere, which is calculated over a few hundred configurations (random position of the impurities inside the nanosphere). The weak variation of ρ_{in} with respect to x_{ns} , indicates that the disappearance of the discreteness in ρ_{in} (as seen in the isolated nanosphere spectrum) results mainly from the interactions between the cluster

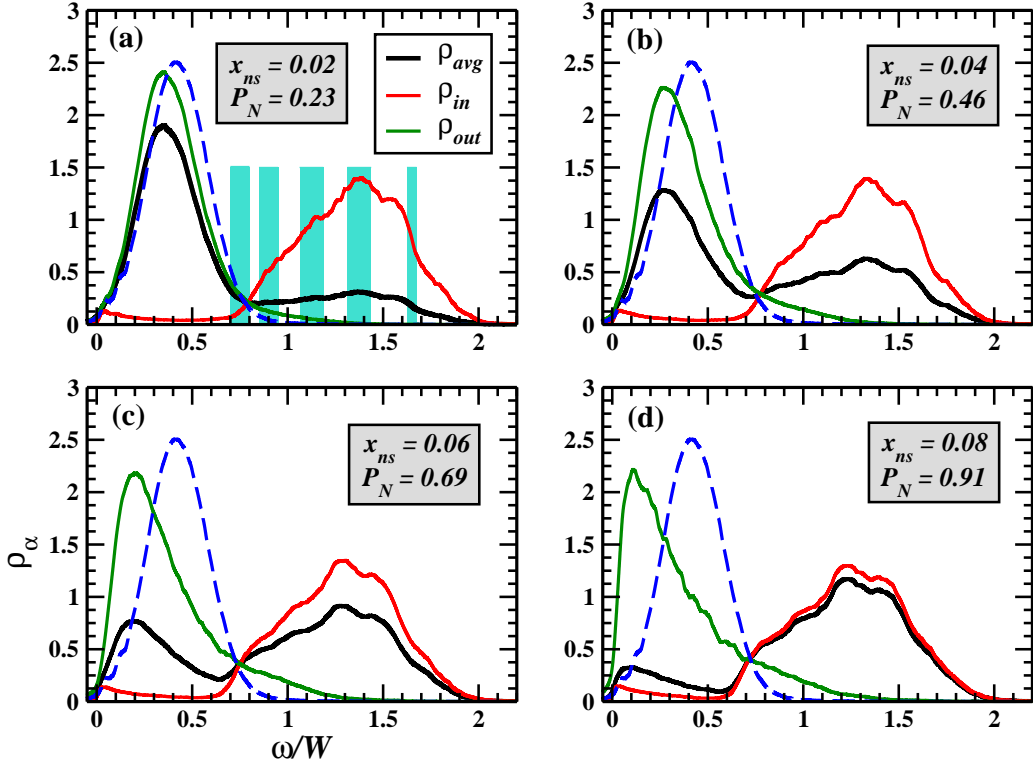


FIG. 2: (Color online) ρ_α denotes the average magnon DOS (ρ_{avg}), local magnon DOS inside (ρ_{in}), and outside the nanospheres (ρ_{out}), for four different x_{ns} . P_N is the percentage of total impurities inside the nanospheres. The blue dashed curves represent the homogeneous ρ_{avg} from Figure 1(a). The shaded regions in (a) correspond to the calculated eigenmodes of a single isolated nanosphere. The parameters are $\lambda=a$, $r_0=2a$, and $x_{in}=0.8$. The x axis is in units of ω/W , where $W \approx 4J_0$ is homogeneous magnon bandwidth.

impurities and those outside. The above discussion of ρ_{avg} and ρ_{in} explains naturally the behavior of ρ_{out} . In the case of more extended couplings, it is expected that (i) ρ_{avg} loses progressively the bimodal nature, (ii) the pseudo-gap in ρ_{in} at low energies is filled gradually, and (iii) the second peak in ρ_{in} becomes narrower and shifts to higher energies with respect to the spectrum of a single isolated cluster.

We now discuss the effects of short ranged interactions ($\lambda=a/2$) on the average and local magnon DOS. The results are shown in Fig. 3. The magnon bandwidth increases by 250% with respect to that of the homogeneous system. As seen before, we observe a clear transfer of weight in ρ_{avg} , from the low to higher energies with increasing x_{ns} . In contrast to

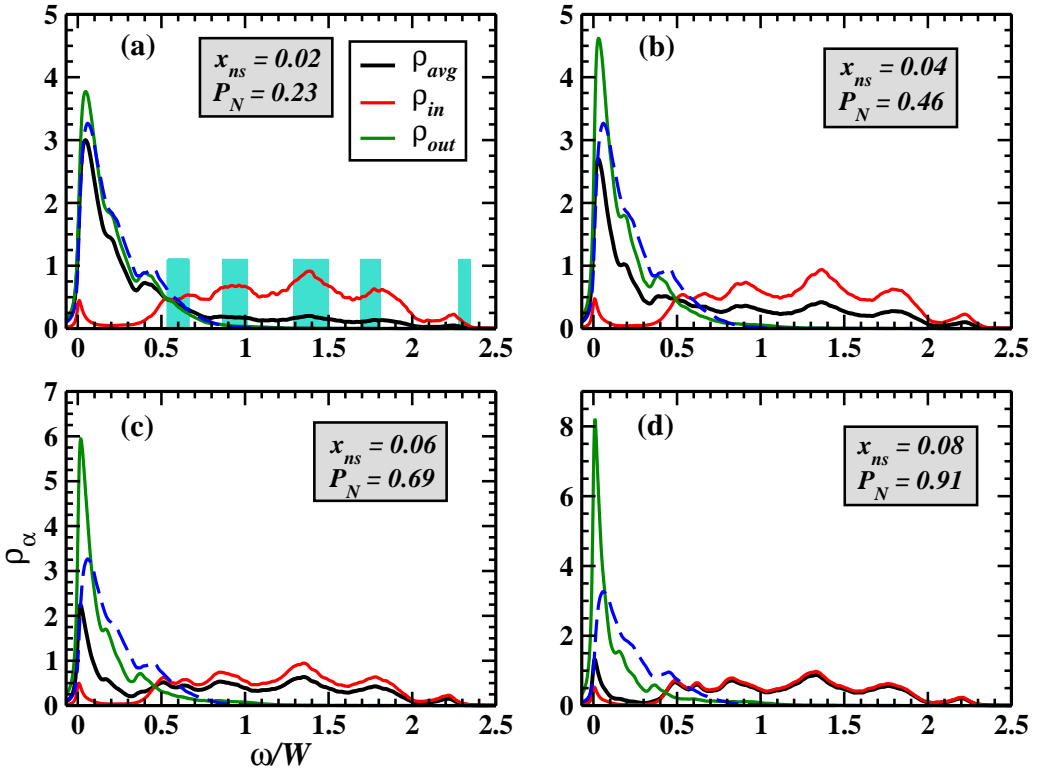


FIG. 3: (Color online) ρ_{avg} , ρ_{in} , and ρ_{out} for $\lambda=a/2$, for four different x_{ns} . The blue dashed curves represent the homogeneous ρ_{avg} from Figure 1(b). The shaded regions in (a) correspond to the calculated eigenmodes of a single isolated nanosphere. The other parameters being same as in Fig. 2. The homogeneous magnon bandwidth is $W \approx 0.8J_0$.

the bimodal nature observed for $\lambda=a$, ρ_{avg} now exhibits a long wavy tail, extending toward higher energies. ρ_{in} shows (i) a clear multiple peak structure now, (ii) is independent of x_{ns} , and (iii) a well defined gap of approximately $0.5W$ is observed. The reasons for the appearance of these multiple peaks in ρ_{in} are the enhanced discreteness (larger sub-gaps) of the eigenmodes of the single isolated nanosphere and the reduced interactions of the cluster impurities with those outside. Concerning ρ_{out} , besides a shift to lower energies as seen for $\lambda=a$, we now observe that the peak becomes narrower with increase in x_{ns} . (The latter feature was absent for the long ranged couplings). The reason for this is with increasing x_{ns} , the concentration of impurities outside decreases and the effective interactions between them become weaker. This effect will be even more pronounced for shorter ranged couplings. Even though the couplings are comparable, drastic changes between Fig. 2 and Fig. 3, shows

that $\lambda=a$ corresponds to the intermediate range couplings and $\lambda=a/2$ definitely to the short range regime. Similar kind of dramatic effects have also been reported on the effects of nanoscale inhomogeneities on critical temperatures²⁷.

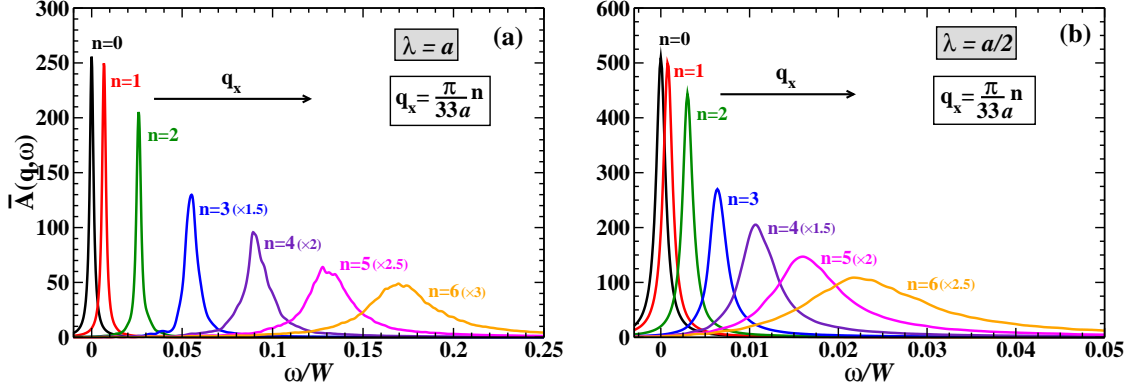


FIG. 4: (Color online) Average spectral function $\bar{A}(\mathbf{q}, \omega)$ as a function of the energy in the (1 0 0) direction for different values of q_x , corresponding to the homogeneous case for (a) $\lambda=a$, and (b) $\lambda=a/2$. The energy axis (x-axis) is in units of ω/W . The system size is $N=66^3$. (The intensity of the peaks have been multiplied by the factors indicated in the parentheses).

We propose now to focus on the low energy excitation spectrum in these systems. For this purpose we evaluate the dynamical spectral function, which provides deeper insight into the underlying spin dynamics. This physical quantity can be directly and accurately probed by inelastic neutron scattering (INS) experiments. It is defined by $\bar{A}(\mathbf{q}, \omega) \equiv \langle A^c(\mathbf{q}, \omega) \rangle_c = -\left\langle \frac{1}{2\pi\langle\langle S^z \rangle\rangle} \text{Im}G^c(\mathbf{q}, \omega) \right\rangle_c$, where $\langle\langle S^z \rangle\rangle = \frac{1}{N_{imp}} \sum_i \langle S_i^z \rangle$ is the total average magnetization over all spin sites, and $G^c(\mathbf{q}, \omega)$ is the Fourier transform of $G_{ij}^c(\omega)$ given in Eq. 2. The averaged dynamical spectral function is evaluated from the following

$$\bar{A}(\mathbf{q}, \omega) = \left\langle \sum_{\alpha} A_{\alpha}^c(\mathbf{q}) \delta(\omega - \omega_{\alpha}^c) \right\rangle_c \quad (4)$$

and

$$A_{\alpha}^c(\mathbf{q}) = \frac{1}{N_{imp}} \sum_{ij} \lambda_j \langle i | \Psi_{\alpha}^{R,c} \rangle \langle \Psi_{\alpha}^{L,c} | j \rangle e^{i\mathbf{q}(\mathbf{r}_i - \mathbf{r}_j)} \quad (5)$$

where $\lambda_j = \frac{\langle S_j^z \rangle}{\langle\langle S^z \rangle\rangle}$ is the temperature dependent local parameter. Note that at $T = 0$ K, all λ_j 's = 1.

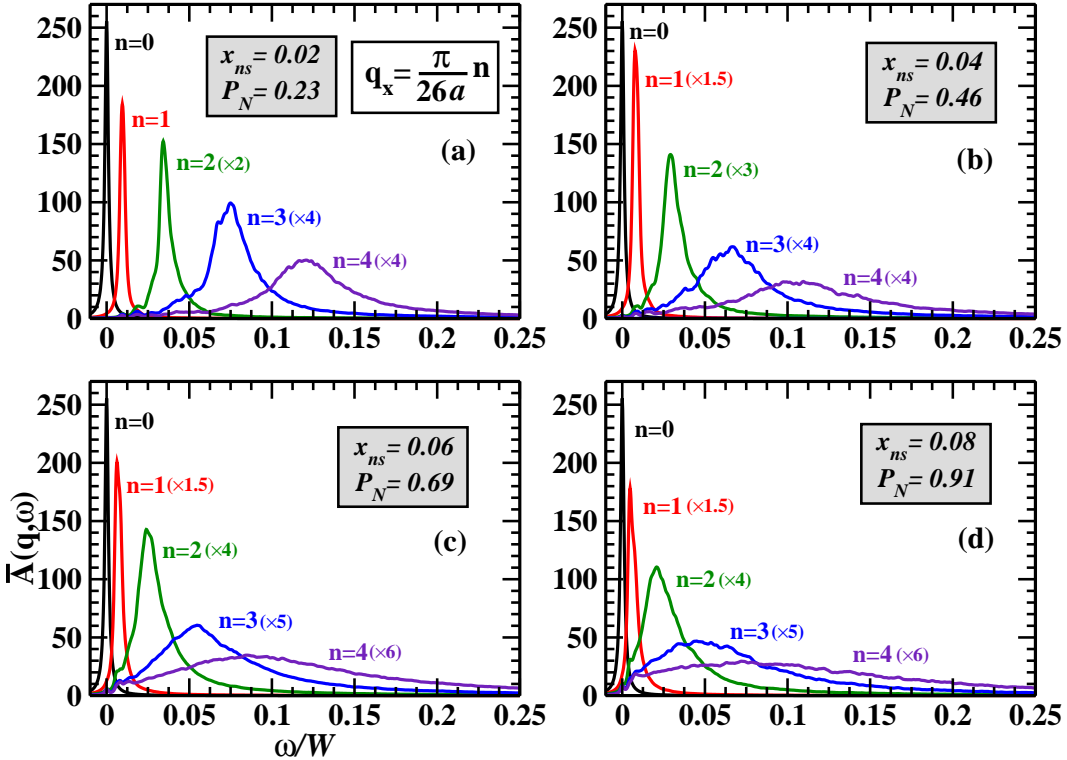


FIG. 5: (Color online) Average spectral function $\bar{A}(\mathbf{q}, \omega)$ as a function of the energy in the $(1 0 0)$ direction, for four different x_{ns} . P_N indicates the percentage of total impurities inside the nanospheres. The parameters are $\lambda=a$, $r_0=2a$, $x_{in}=0.8$, and $N=52^3$. The x axis is in units of ω/W . (The intensity of the peaks have been multiplied by the factors indicated in the parentheses).

We start with the average spectral function for the homogeneously diluted systems. Figs. 4(a) and 4(b) show $\bar{A}(\mathbf{q}, \omega)$, for $\lambda=a$ and $a/2$ respectively, as a function of the energy for different values of the momentum \mathbf{q} in the $(1 0 0)$ direction. First in both cases, as q increases the peaks become broader and more asymmetric with a tail extending toward higher energies. Well-defined excitations exist only for relatively small values of the momentum, beyond $q_x a \approx 0.24\pi$ no well-defined magnons exist. However, for $\lambda=a$, the well-defined excitations persist up to energy values of about $0.25W$, whilst for $\lambda=a/2$ the excitations reaches only up to $0.035W$, where W is the λ -dependent magnon spectrum bandwidth. We remind that $W \approx 4J_0$ and $0.8J_0$, for $\lambda=a$ and $a/2$, respectively.

We now proceed further and analyze the effects of nanoscale inhomogeneities on the dynamical spectral function. The results for $\lambda=a$ are depicted in Fig. 5. As we increase

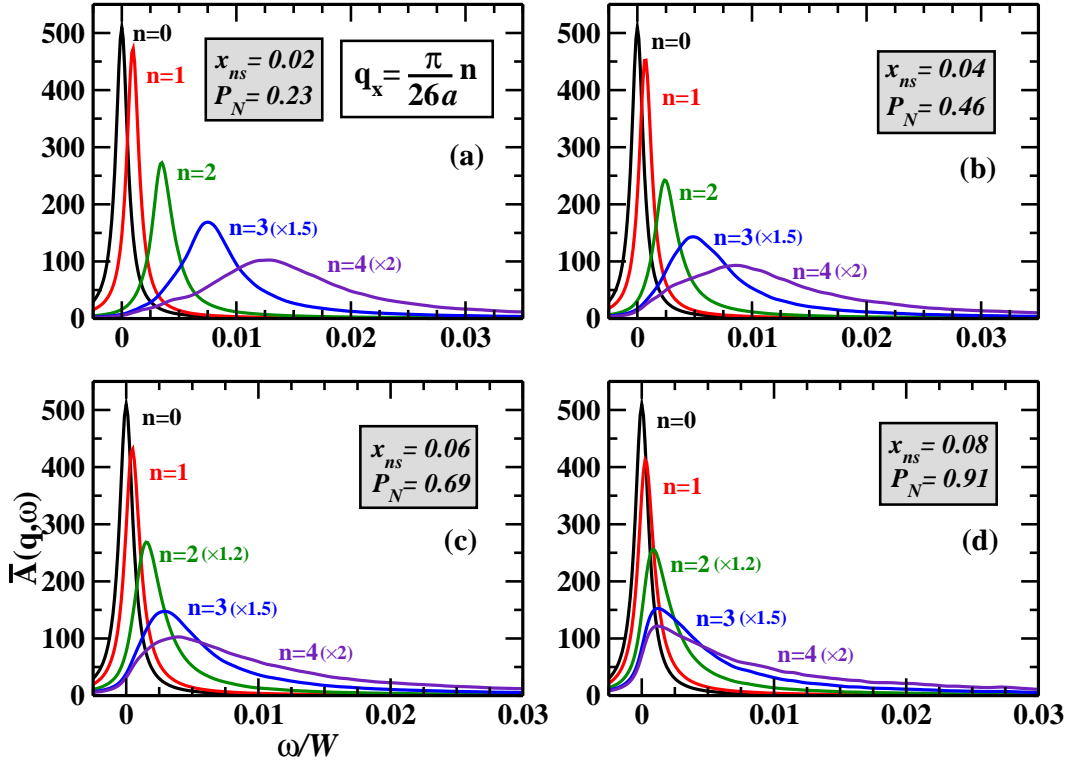


FIG. 6: (Color online) Average spectral function $\bar{A}(\mathbf{q}, \omega)$ for the case of $\lambda=a/2$, with the other parameters same as in Fig. 5.

x_{ns} , there is a broadening in the excitations, accompanied with an increase in asymmetry and a shift toward the lower energies is observed. These effects are already pronounced even for the lowest concentration of nanospheres. For instance, for $q_x a \approx 0.12\pi$, the magnon energies are $0.09W$, $0.075W$, and $0.067W$, for $x_{ns}=0$, 0.02 , and 0.04 , respectively. In order to analyze the effects of inhomogeneities on the magnon lifetime for a given \mathbf{q} , we define the ratio $R(\mathbf{q}) = \gamma(\mathbf{q})/\omega(\mathbf{q})$, where $\gamma(\mathbf{q})$ is the half-width of the excitations. The excitations are well-defined in character only when $R(\mathbf{q}) < 1$. For the aforesaid q_x , the corresponding $R(\mathbf{q})$'s are 0.2 , 0.33 , and 0.66 , for $x_{ns}=0$, 0.02 , and 0.04 , which corresponds to an increase of about 60% and 200% respectively, compared to the homogeneous case, for these two values of x_{ns} . It is interesting to note that these effects could hardly be anticipated from the magnon DOS results (Fig. 2). In fact the analyses of the DOS suggested that the low energy excitations should be weakly affected by the inhomogeneities. In the following, we discuss the spectral function in the presence of short-ranged interactions, shown in Fig. 6. As in the previous

case, well-defined excitations exist only for small values of the momentum. However, here we find that the shift toward the lower energies is strongly enhanced. If we consider the particular case of $q_x a \approx 0.12\pi$, the magnon energies are shifted by 30% and 60% respectively, for $x_{ns}=0.02$ and 0.04, with respect to that of the homogeneous case. The $R(\mathbf{q})$'s for this value of q_x are 0.4, 0.8, and 1.3 for $x_{ns}=0$, 0.02, and 0.04. This indicates that the excitations have dramatically lost their well defined character as compared to the previous case (Fig. 5).

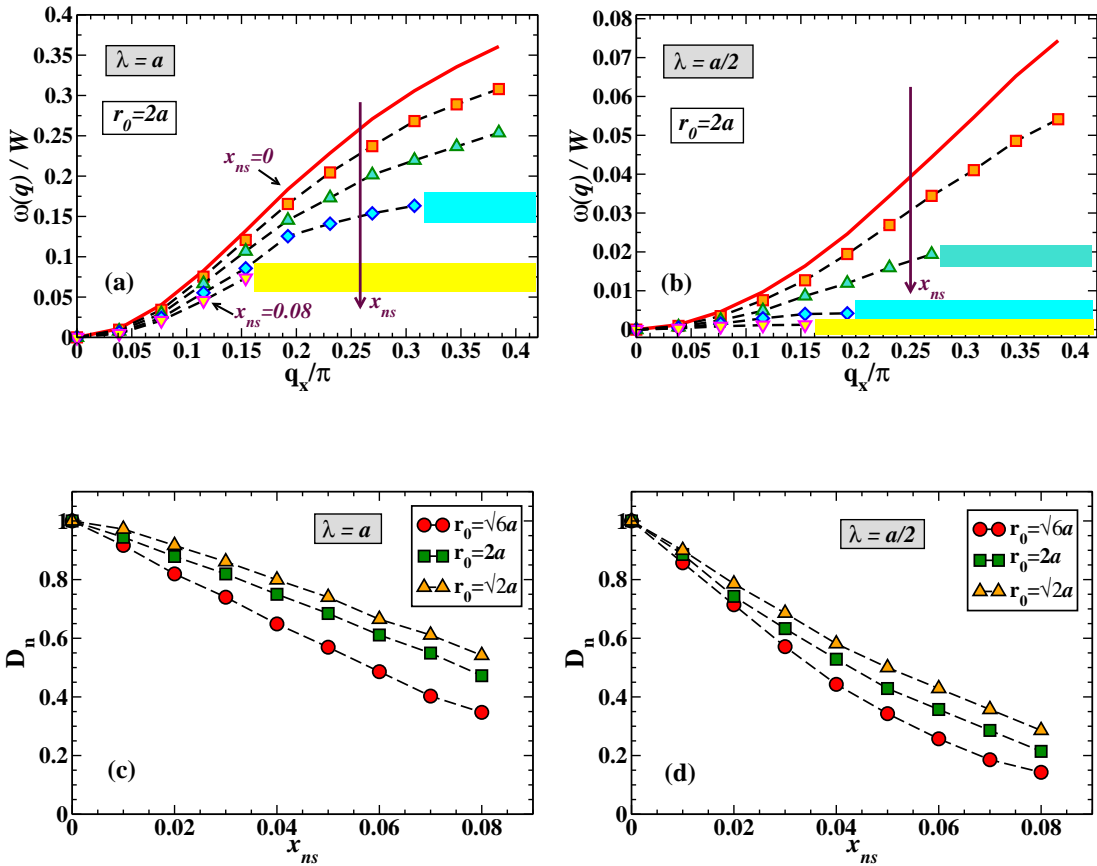


FIG. 7: (Color online) Magnon dispersion as a function of q_x/π , for different x_{ns} (0, 0.02, 0.04, 0.06, and 0.08) for (a) $\lambda=a$, and (b) $\lambda=a/2$. The vertical arrows indicate the direction of increasing x_{ns} . The solid (red) curve corresponds to the homogeneous case. The shaded regions indicate the q values beyond which there is no clear maxima in the magnon excitations. (c) and (d) show the normalized spin-stiffness D_n as a function of x_{ns} , corresponding to $\lambda=a$, and $\lambda=a/2$, respectively, for three different r_0 : $\sqrt{6}a$, $2a$, and $\sqrt{2}a$. The concentration inside nanospheres is $x_{in}=0.8$.

From the $\bar{A}(\mathbf{q}, \omega)$ calculations, we now extract both the magnon dispersion $\omega(\mathbf{q})$ and the

spin-stiffness D^{inh} . We remind that in the long wavelength limit, $\omega(\mathbf{q})=D^{inh}q^2$. In order to gauge the effects of the inhomogeneities, we define the normalized spin-stiffness coefficient $D_n=D^{inh}/D^{hom}$, where D^{inh} denotes the spin-stiffness of the inhomogeneous systems, and D^{hom} that of the homogeneously diluted system. The values of the spin-stiffness D^{hom} are found to be $2.9J_0$ and $0.07J_0$, for $\lambda=a$ and $a/2$ respectively, for $x=0.07$. We would like to stress that both $\omega(\mathbf{q})$ and D^{inh} were obtained from the first non-zero \mathbf{q} excitations ($\mathbf{q}=(\frac{2\pi}{La}, 0, 0)$) corresponding to system sizes $N = L^3$, where L varies from 36 to 52. Figs. 7(a) and 7(b) show $\omega(\mathbf{q})$ as a function of \mathbf{q} for various x_{ns} , corresponding to $\lambda=a$, and $a/2$ respectively. First, in both cases, we observe that the inhomogeneities suppress the magnon dispersion. This suppression is even more drastic in the case of short-ranged interactions. In addition, the quadratic behavior persists up to large \mathbf{q} for $\lambda=a/2$, whilst a clear softening of the magnon modes can be seen in the case of the extended couplings, for $q_x/\pi \geq 0.2$. This is consistent with the discussions of Figs. 5 and 6. The well-defined magnon region shrinks significantly on going from $\lambda=a$ to $\lambda=a/2$. This tendency is enhanced on increasing x_{ns} . In order to evaluate more quantitatively the effects of the inhomogeneities, the normalized spin-stiffness D_n is plotted in Figs. 7(c) and 7(d), as a function of x_{ns} , for various radii of the nanospheres. As anticipated from the previous figures, one observes for both $\lambda=a$ and $a/2$, a monotonous decrease of the spin-stiffness with increasing x_{ns} . D_n decreases almost linearly up to $x_{ns} \approx 0.04$. The slope for $\lambda=a/2$ is twice that of $\lambda=a$. We find that the suppression of the spin-stiffness is greater for larger radii of the nanospheres. For instance, for the particular $x_{ns}=0.03$, the spin-stiffness is reduced by 15% for $r_0=\sqrt{2}a$, and by almost 30% for $r_0=\sqrt{6}a$, for $\lambda=a$ (Fig. 7(c)), although the concentration outside the nanospheres is almost the same. In the case of the short-ranged couplings this effect is even stronger. The effects of the nanoscale inhomogeneities on the spin-stiffness are in striking contrast to that observed on the critical temperatures, where an increase by more than one order of magnitude was found²⁷.

To conclude, in this work we have shed light on the effects of nanoscale inhomogeneities on the magnetic excitation spectrum of dilute systems. To our knowledge, no such detailed numerical study has been performed so far. Compared to homogeneously diluted systems, even low concentrations of nanoscale inhomogeneities is sufficient to induce drastic changes in the magnon DOS. The magnon dispersion is found to vary significantly with the concentration of inhomogeneities, leading to a strong suppression of the spin-stiffness. This is in

contrast to what has been reported about the critical temperatures. We also find a strong increase of the half-width of the magnon excitations in the long wavelength limit. These features are strongly enhanced in the case of short-ranged couplings. Now it would be interesting to study the effects of temperature on the spin dynamics of these inhomogeneous systems⁴⁶. We expect the temperature dependence of the spin-stiffness, especially in systems with short-ranged interactions, to be unconventional compared to that of the homogeneous systems. Finally, we believe this detailed study would serve to motivate future experimental works on these inhomogeneous compounds.

Acknowledgments

This work was supported by the EU within FP7-PEOPLE-ITN-2008, Grant number 234970 Nanoelectronics: Concepts, Theory and Modelling.

- ¹ V. L. Moruzzi, Phys. Rev. B **41**, 6939 (1990).
- ² I. A. Abrikosov, O. Eriksson, P. Söderlind, H. L. Skriver, and B. Johansson, Phys. Rev. B **51**, 1058 (1995).
- ³ P. James, O. Eriksson, B. Johansson, and I. A. Abrikosov, Phys. Rev. B **59**, 419 (1999).
- ⁴ T. Jungwirth, J. Sinova, J. Masek, J. Kucera, and A. H. MacDonald, Rev. Mod. Phys. **78**, 809 (2006).
- ⁵ K. Sato, L. Bergqvist, J. Kudrnovský, P. H. Dederichs, O. Eriksson, I. Turek, B. Sanyal, G. Bouzerar, H. Katayama-Yoshida, V. A. Dinh, T. Fukushima, H. Kizaki, and R. Zeller, Rev. Mod. Phys. **82**, 1633 (2010).
- ⁶ C. Timm, J. Phys. Condens. Matter **15**, R1865 (2003).
- ⁷ T. Fukumura, H. Toyosaki, and Y. Yamada, Semicond. Sci. Technol. **20**, S103 (2005).
- ⁸ S. A. Chambers, T. C. Droubay, C. M. Wang, K. M. Rosso, S. M. Heald, D. A. Schwartz, K. R. Kittilstved, and D. R. Gamelin, Mater. Today **9**, 28 (2006).
- ⁹ M. B. Salamon and M. Jaime, Rev. Mod. Phys. **73**, 583 (2001).
- ¹⁰ T. Goto, T. Kimura, G. Lawes, A. P. Ramirez, and Y. Tokura, Phys. Rev. Lett. **92**, 257201 (2004).

¹¹ E. Dagotto, *Nanoscale Phase Separation and Colossal Magnetoresistance* (Springer-Verlag, Berlin, Germany, 2002).

¹² K. W. Edmonds, K. Y. Wang, R. P. Campion, A. C. Neumann, N. R. S. Farley, B. L. Gallagher, and C. T. Foxon, *Appl. Phys. Lett.* **81**, 4991 (2002).

¹³ K. C. Ku, S. J. Potashnik, R. F. Wang, S. H. Chun, P. Schiffer, N. Samarth, M. J. Seong, A. Mascarenhas, E. Johnston-Halperin, R. C. Meyers, A. C. Gossard, and D. D. Awschalom, *Appl. Phys. Lett.* **82**, 2302 (2003).

¹⁴ R. Bouzerar and G. Bouzerar, *Europhys. Lett.* **92**, 47006 (2010).

¹⁵ M. Moreno, A. Trampert, B. Jenichen, L. Däweritz, K. H. Ploog, *J. Appl. Phys.* **92**, 4672 (2002).

¹⁶ M. Yokoyama, H. Yamaguchi, T. Ogawa, and M. Tanaka, *J. Appl. Phys.* **97**, 10D317 (2005).

¹⁷ F. Xiu, Y. Wang, J. Kim, A. Hong, J. Tang, A. P. Jacob, J. Zou, and K. L. Wang, *Nat. Mater.* **9**, 337 (2010).

¹⁸ D. Bougeard, S. Ahlers, A. Trampert, N. Sircar, and G. Abstreiter, *Phys. Rev. Lett.* **97**, 237202 (2006).

¹⁹ Y. D. Park, A. Wilson, A. T. Hanbicki, J. E. Mattson, T. Ambrose, G. Spanos, and B. T. Jonker, *Appl. Phys. Lett.* **78**, 2739 (2001).

²⁰ N. Jedrecy, H. J. von Bardeleben, and D. Demaille, *Phys. Rev. B* **80**, 205204 (2009).

²¹ M. Fäth, S. Freisem, A. A. Menovsky, Y. Tomioka, J. Aarts, and J. A. Mydosh, *Science* **285**, 1540 (1999).

²² R. von Helmholz, J. Wecker, B. Holzapfel, L. Schultz, and K. Samwer, *Phys. Rev. Lett.* **71**, 2331 (1993).

²³ S. Jin, T. H. Tiefel, M. McCormack, R. A. Fastnacht, R. Ramesh, and L. H. Chen, *Science* **264**, 413 (1994).

²⁴ S. H. Pan, J. P. O’Neal, R. L. Badzey, C. Chamon, H. Ding, J. R. Engelbrecht, Z. Wang, H. Eisaki, S. Uchida, A. K. Gupta, K. W. Ng, E. W. Hudson, K. M. Lang, and J. C. Davis, *Nature* **413**, 282 (2001).

²⁵ W. D. Wise, K. Chatterjee, M. C. Boyer, T. Kondo, T. Takeuchi, H. Ikuta, Z. Xu, J. Wen, G. D. Gu, Y. Wang, and E. W. Hudson, *Nat. Phys.* **5**, 213 (2009).

²⁶ C. V. Parker, A. Pushp, A. N. Pasupathy, K. J. Gomes, J. Wen, Z. Xu, S. Ono, G. Gu, and A. Yazdani, *Phys. Rev. Lett.* **104**, 117001 (2010).

²⁷ A. Chakraborty, R. Bouzerar, S. Kettemann, and G. Bouzerar, Phys. Rev. B **85**, 014201 (2012).

²⁸ Y. Motome and N. Furukawa, Phys. Rev. B **71**, 014446 (2005).

²⁹ J. Zhang, F. Ye, H. Sha, P. Dai, J. A. Fernandez-Baca, and E. W. Plummer, J. Phys.: Condens. Matter **19**, 315204 (2007).

³⁰ D. Louca and J. L. Sarrao, Phys. Rev. Lett. **91**, 155501 (2003).

³¹ M. J. R. Hoch, P. L. Kuhns, W. G. Moulton, A. P. Reyes, J. Wu, and C. Leighton, Phys. Rev. B **69**, 014425 (2004).

³² M. Poienar, F. Damay, C. Martin, J. Robert, and S. Petit, Phys. Rev. B **81**, 104411 (2010).

³³ J. T. Haraldsen, F. Ye, R. S. Fishman, J. A. Fernandez-Baca, Y. Yamaguchi, K. Kimura, and T. Kimura, Phys. Rev. B **82**, 020404(R) (2010).

³⁴ T. A. Maier and D. J. Scalapino, Phys. Rev. B **78**, 020514(R) (2008).

³⁵ R. A. Ewings, T. G. Perring, R. I. Bewley, T. Guidi, M. J. Pitcher, D. R. Parker, S. J. Clarke, and A. T. Boothroyd, Phys. Rev. B **78**, 220501(R) (2008).

³⁶ Y. J. Uemura and R. J. Birgeneau, Phys. Rev. Lett. **57**, 1947 (1986); Y. J. Uemura and R. J. Birgeneau, Phys. Rev. B **36**, 7024 (1987).

³⁷ More details on bi-orthogonality can be found in J. Dieudonné, Mich. Math. J. **2**, 7 (1953).

³⁸ G. Bouzerar, T. Ziman, and J. Kudrnovský, Europhys. Lett. **69**, 812 (2005).

³⁹ G. Bouzerar, Eur. Phys. Lett. **79**, 57007 (2007).

⁴⁰ A. Chakraborty and G. Bouzerar, Phys. Rev. B **81**, 172406 (2010).

⁴¹ A. Chakraborty, R. Bouzerar, and G. Bouzerar, Eur. Phys. J. B **81**, 405 (2011).

⁴² S.T.B. Goennenwein et al., Appl. Phys. Lett. **82**, 730 (2003).

⁴³ M. Sperl et al., Phys. Rev. B **77**, 125212 (2008).

⁴⁴ L. Bergqvist, O. Eriksson, J. Kudrnovský, V. Drchal, P. Korzhavyi and I. Turek, Phys. Rev. Lett. **93**, 137202 (2004).

⁴⁵ K. Sato, W. Schweika, P. H. Dederichs and H. Katayama-Yoshida, Phys. Rev. B **70**, 201202(R) (2004).

⁴⁶ A. Chakraborty *et. al.*, unpublished.